Title
Continuous pervaporation-assisted furfural production catalyzed by CrCl 3

Journal
Green Chemistry, 20(12)

ISSN
1463-9262

Authors
Wang, Alex
Balsara, Nitash P
Bell, Alexis T

Publication Date
2018

DOI
10.1039/c8gc00842f

Peer reviewed

Green Chemistry

PAPER

View Article Online
View Journal | View Issue

Cite this: *Green Chem.*, 2018, **20**, 2903

Continuous pervaporation-assisted furfural production catalyzed by $CrCl_3$†

Alex Wang, [a,b] Nitash P. Balsara [*a,b,c] and Alexis T. Bell [*a,b]

Received 15th March 2018,
Accepted 24th May 2018

DOI: 10.1039/c8gc00842f

rsc.li/greenchem

Furfural—a precursor to fuels, solvents, and polymers—is produced by acid-catalyzed dehydration of biomass-derived xylose; however, the selectivity of this process is limited by side reactions which form low-value byproducts known as humins. The production of humins can be reduced by extracting furfural as it is produced. In this paper we report the design and performance of a membrane-pervaporation-assisted reactor for the continuous $CrCl_3$-catalyzed conversion of xylose to furfural. Pervaporation offers a simple means for separating products from homogeneous catalysts and reactants with negligible vapor pressure. By combining reaction with product pervaporation, it was possible to produce furfural continuously without catalyst addition during the reaction. We also conducted simulations of the continuous reaction while varying the membrane-area-to-reactor-volume ratio, a_v. These simulations showed that there is an optimal value of a_v for which the permeate concentration of furfural and reaction selectivity are maximized. For the parameters used in this study, the optimal value of a_v is 0.17 cm^{-1}. Our work provides a basis for the design of a continuous pervaporation-assisted reactor and illustrates the sensitivity of this approach to individual system parameters.

Introduction

Furfural is a versatile, biomass-derived platform chemical.[1–3] Recent developments have demonstrated that it can be used for the production of fuels,[4–8] solvents,[9–12] polymers,[3,11–14] and pharmaceuticals.[1,12,15] Current furfural production is about 300 kton per annum and mostly comes from China, although the Dominican Republic and South Africa also produce furfural on a large scale.[3,7,16,17]

Modern furfural production is carried out in both batch and continuous reactors, which are typically loaded with about 25–33 wt% lignocellulosic biomass (*e.g.* oat hulls, corn cobs, and bagasse)[16] and 3 wt% sulfuric acid (H_2SO_4) and then heated with steam (25–35 tons of steam per ton of furfural produced).[7,16] The reaction is carried out at temperatures of 180–250 °C.[3,7,16,18] H_2SO_4 serves as the catalyst to promote depolymerization of polysaccharides present in the biomass to yield monosaccharides. Five-carbon monosaccharides, *e.g.* xylose, subsequently undergo dehydration promoted by the same catalyst to produce furfural. The steam not only heats the reactors, but also extracts furfural as it is produced. This steam-stripping process mitigates the formation of low-value byproducts known as humins, which form by coupling of xylose or furfural with reaction intermediates and by resinification of furfural.[18–20] A limitation of this process is that it produces only 40–70% of the theoretical yield of furfural.[1,3,7,16]

Researchers have recently explored the use of liquid–liquid extraction (LLE) with an immiscible organic solvent in laboratory-scale, biphasic, batch reactors, rather than steam, to improve furfural yield. These reactors are typically operated at temperatures of 130–180 °C.[21–31] Solvents include toluene,[21–24] methyl isobutyl ketone,[23–26] cyclopentylmethyl ether,[27–29] among others, and are typically used in organic : aqueous volumes ratios greater than 1 in order to increase furfural extraction. The furfural yield depends on solvent, catalyst, xylose loading, *etc.* and is increased relative to an equivalent reaction without extraction by as much as 100%.[25]

Our objective is to present a new membrane reactor for continuous production of furfural from xylose. Furfural produced by reaction is separated using pervaporation through a non-porous membrane, a technique shown to extract furfural from water selectively.[32–40] We conducted experiments at 90 °C (within the temperature limits of the membranes) with chromium(III) chloride ($CrCl_3$) as a homogeneous catalyst, since $CrCl_3$ has previously been shown to convert xylose to furfural rapidly.[30,31,41] This study builds on our previous investigations, which demonstrated the performance of a batch membrane reactor for producing furfural from xylose using a hetero-

[a]*Department of Chemical and Biomolecular Engineering, University of California, Berkeley, CA 94720, USA. E-mail: alexbell@berkeley.edu, nbalsara@berkeley.edu*
[b]*Energy Biosciences Institute, University of California, Berkeley, CA 94704, USA*
[c]*Material Sciences Division and Environmental Energy Technologies Division, Lawrence Berkeley National Laboratory, Berkeley, CA 94720, USA*

†Electronic supplementary information (ESI) available. See DOI: 10.1039/c8gc00842f

geneous catalyst.[40] Here, we combine the reaction and membrane processes thereby eliminating the extraneous heating and cooling elements of the prior membrane reactor design in order to achieve a system that can be used for continuous reaction and separation. We found that pervaporation is able to fully retain the homogeneous catalyst in the reactor. This is significant because H_2SO_4, a homogeneous catalyst, is pervasive in industrial furfural production and must be constantly fed into the reactor.[3,7,16,18] Our continuous reactor requires no input of homogeneous catalyst beyond the initial charge—much like a continuous, heterogeneously catalyzed process—implying that homogenous catalyst addition could be reduced in an industrial-scale process. It is also worth noting that homogeneous catalysts may produce furfural with higher selectivity when compared to heterogeneous catalysts,[42] but to the authors' knowledge a broad comparison of homogeneous catalysts with their analogous heterogeneous counterparts has not been explored for furfural production. Our experimental results were then used to develop a model for simulating reactor performance as a function of membrane surface area. Surprisingly, we found that the permeate concentration of product and the reaction selectivity are maximized by choice of the membrane-surface-area-to-reactor-volume ratio, a_v.

Experimental methods

Materials

D-(+)-Xylose (99%), D-(−)-lyxose (99%), D-xylulose (98%), furfural (99%), toluene (99.5%), dodecane (99%), cyclohexane (99%), and chromium(III) chloride hexahydrate ($CrCl_3$; 98.0%) were purchased from Sigma-Aldrich and used as received. Sulfuric acid (H_2SO_4; 95%) was purchased from Acros Organic and was used as received. Nanopure water was used for all experiments. Cross-linked polydimethylsiloxane (PDMS) thin-film composite membranes were purchased from Pervatech and had a 130 μm-thick polyethylene terephthalate support layer, a 100 μm-thick polyisoprene intermediate ultrafiltration membrane layer, and a 3–5 μm-thick pervaporation PDMS layer (4 μm was used in all calculations requiring membrane thickness). These membranes were received as sheets and were cut to fit the membrane cell. The block copolymer polystyrene-*block*-polydimethylsiloxane-*block*-polystyrene (SDS), which was previously shown to be permeable to furfural,[38–40] was purchased from Polymer Source and was used as received. The number-averaged molecular weight of the polydimethylsiloxane block was 104 kg mol^{-1}, and that of each polystyrene block was 22 kg mol^{-1}. The dispersity of the polymer sample was 1.3, and 86 wt% of the sample was the triblock copolymer with the balance being mostly diblock copolymer.

SDS membrane preparation

A solution consisting of 0.5–1 g of SDS dissolved in 20 mL of cyclohexane was used to prepare each solvent-cast SDS membrane. The solution was poured onto a 100 mm polytetrafluoroethylene (PTFE) evaporation dish (Fisher, 02-617-148), which was then covered and allowed to dry in a fume hood for three days. The resulting membrane was peeled off the dish, sandwiched between two filter papers, and cut to fit the pervaporation cell. The thickness of each solvent-cast membrane was measured at 12 points using a micrometer and the average value was used in all calculations involving membrane thickness.

Furfural production at 90 °C with or without pervaporation

Reactions at 90 °C were carried out in a custom-built apparatus, shown schematically in Fig. 1. This reactor was comprised of a membrane-reactor cell, a magnetic stir plate (Thermo Scientific, 88880013), two cold traps for condensing permeated vapors, a vacuum pump (Welch, 2014), a high-pressure nitrogen cylinder (Praxair, NI 2R), a gas pressure regulator (VWR, 55850-624), and an 800 mL feed reservoir (EMD Millipore, 6028). The components were connected by stainless steel (Swagelok), polyethylene (PE; EMD Millipore), polytetrafluoroethylene (PTFE; Grainger), and silicone (Cole-Parmer) tubing; and stainless steel (Swagelok), PE (EMD Millipore), and polyether ether ketone (PEEK; IDEX Health & Science) fittings and valves.

The membrane cell had three main components: a head, a base, and a glass tube. The head was fabricated from PEEK and had four attachments: a thermocouple (Omega, TMTSS-062G-6), a pressure relief valve (General Air Products, ST12), a sampler, and an inlet tube from the feed reservoir. Corrosion was prevented by placing the thermocouple in a glass sheath and electroplating the relief valve with gold. Additionally, a shaft carrying a PTFE-coated magnetic stir bar and bearing extended from the head into the membrane cell, suspending the stir bar 5 mm above the membrane surface. The base was a circular piece of gold-electroplated stainless steel, containing a 4.8 cm-diameter circular recess into which the membrane was placed. The recess had grooves cut into it

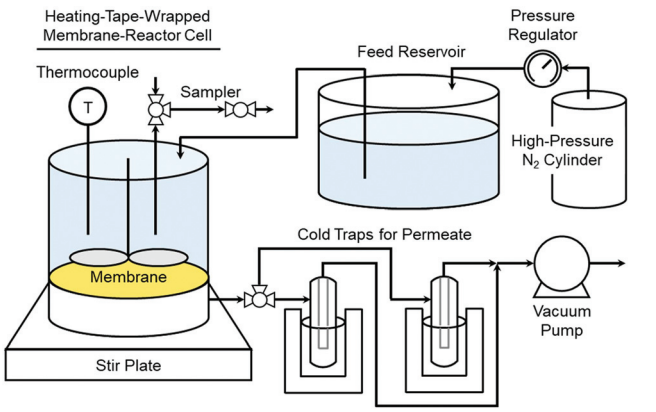

Fig. 1 Pervaporation membrane reactor. Reaction takes place at 90 °C in the 83 mL cell, while furfural is continuously extracted by the pervaporation membrane. The nitrogen cylinder, pressure regulator, and feed reservoir maintain constant liquid volume in the cell. The vacuum pump enables pervaporation, while the cold traps collect permeated vapors (*i.e.*, furfural and water).

to facilitate permeate flow from the membrane through a silicone tube in the base that led to the cold traps. The glass tube served as the walls of the membrane cell and was a piece of borosilicate glass wrapped in heating tape (Omega, STH051-020). The temperature was controlled by a controller (Omega, CNi3233), which was connected to the thermocouple and heating tape. Viton O-rings (42 × 3 mm, McMaster-Carr, 9263K736) were placed on both ends of the glass tube, resulting in a membrane area of 13.9 cm^2. The cell was assembled by placing, from top to bottom, the head, an O-ring, the tube, an O-ring, the membrane, a piece of filter paper, and the base. The head, glass tube, and base were sealed by screwing bolts onto three posts that ran from the base to the head, providing compression to the O-rings. The cell was then placed on top of a magnetic stir plate. The internal volume of the cell was 83 mL and it was always filled to that amount during use.

Two cold traps and a vacuum pump were located downstream of the membrane cell. Two sizes of cold traps were used to accommodate the permeation rate, depending on the membrane: small (ChemGlass, CG-4516-02) with the SDS membranes, or large (custom blown by Research & Development Glass Products & Equipment, Berkeley, CA) with the PDMS membrane. Permeate vapors were condensed in the cold traps by cooling them with a dry ice and isopropanol mixture (small) or liquid nitrogen (large). The cold traps were connected to the membrane and vacuum pump in parallel, ensuring that the membrane and vacuum pump were always connected, even when a used cold trap was exchanged for a new one. The vacuum pump was capable of pulling different pressures, depending on the cold traps: ≤3 mbar (small cold traps) or 6–15 mbar (large cold traps), as measured by a vacuum gauge (Vacuubrand, DVR 2) located between the pump and the cold traps.

A high-pressure nitrogen cylinder, gas pressure regulator, and a feed reservoir were located upstream of the membrane cell. The nitrogen cylinder and regulator were connected to the vapor headspace of the feed reservoir, while the feed reservoir was connected to the membrane cell by a dip tube submerged in the liquid of the reservoir. The regulator was used to maintain a gauge pressure of 1 bar throughout the system—a pressure in excess of the vapor pressure of the contents of the membrane cell. During operation, this system was able to sustain a constant liquid volume in the membrane cell, confirmed by measuring the volume of liquid in the cell before and after each experiment. This control mechanism operates as follows. When liquid permeates through the membrane, the cell headspace volume increases and the system pressure drops. The regulator then reacts to this pressure drop by adding more nitrogen to the reservoir headspace to raise the pressure to its setpoint, which pushes liquid through the reservoir dip tube into the cell. Ultimately, the volume of liquid passed through the membrane is replaced by the same volume of liquid from the reservoir.

At the start of each experiment, the membrane cell was assembled with a new membrane: SDS, PDMS, or 130 μm-thick impermeable PTFE for the reaction without pervaporation. The membrane and the cold traps were then connected to each other and evacuated. The catalyst and xylose concentrations were chosen to produce furfural at a rate comparable to the furfural pervaporation rates achievable by the membranes. The cell was filled with 83 mL of an aqueous xylose and $CrCl_3$ solution: 25 μmol mL^{-1} $CrCl_3$ and either 250 μmol mL^{-1} xylose in the batch reactions or 200 μmol mL^{-1} xylose in the continuous reaction. The feed-reservoir liquid was water in the batch reactions with pervaporation, and a solution of 100 g L^{-1} xylose in water for the continuous reaction with pervaporation. The reservoir contained only nitrogen in the batch reaction without pervaporation. The feed reservoir was connected to the cell and the system was pressurized to 1 bar (gauge). The valve connecting the membrane to the cold traps was closed at this point in the batch reaction without pervaporation. Stirring at 600 rpm then began, followed by heating to 90 °C. The cell reached 88 °C within 15 min and 90 °C within 30 min.

The membrane cell was sampled during the reaction using the sampling port, first taking a sample to flush the sampling port, then taking another for analysis. The total volume removed per sample was 800 μL. The permeate was collected at the same time as the reactor was sampled. The permeate flow was directed from the accumulating cold trap to the other installed cold trap (*e.g.*, from the left cold trap to the right one in Fig. 1), then the accumulated cold trap was removed, thawed, and replaced with a fresh one. The thawed permeate was a single-phase mixture under the conditions used in this study. The accumulated cold trap was weighed and diluted with nanopure water and an aliquot was removed for analysis.

Product analysis

Samples were analyzed by high-performance liquid chromatography (HPLC) using an Ultra High Performance Liquid Chromatograph system (Shimadzu). 10 μL aliquots of the samples were injected onto a 300 mm × 7.8 mm Aminex HPX-87H (Bio-Rad) column equipped with a 4.6 mm × 30 mm micro-guard Cation H guard column (Bio-Rad) and a refractive index detector. The compounds were eluted at 65 °C with an isocratic flow rate of 0.4 mL min^{-1} of 0.01 N H_2SO_4 in water. Product quantities were determined by converting integrated peak areas into concentrations using a 7-point calibration curve generated from standards created with analytical grade chemicals.

Permeate samples were additionally analyzed by inductively coupled plasma optical emission spectrometry (ICP-OES) using an Optima 7000 DV instrument with yttrium as an internal standard to determine the presence of chromium. The instrument had a detection limit of 0.25 μg L^{-1} (ppb).

Calculations

For batch reactions, conversions and yields are reported as molar percentages relative to the initial moles of reactant. $CrCl_3$ is capable of isomerizing xylose to form lyxose and xylulose, and of dehydrating all three xylose isomers to form furfural. Conversion of all three isomers in aggregate was

reported as "xylose conversion" rather than the conversion of xylose alone, *i.e.*

$$\text{Xylose Conversion} = \frac{N^0_{\text{xylose}} - (N_{\text{xylose}} + N_{\text{lyxose}} + N_{\text{xylulose}})}{N^0_{\text{xylose}}} \times 100\% \quad (1)$$

where N denotes the moles, the superscript 0 denotes initial value, and the subscript denotes the compound. Similarly, for the reactions which assessed the rate of furfural conversion without any sugars present, furfural conversion was calculated as follows:

$$\text{Furfural Conversion} = \frac{N^0_{\text{furfural}} - N_{\text{furfural}}}{N^0_{\text{furfural}}} \times 100\% \quad (2)$$

The product of interest in this study was furfural and its yield was defined as

$$\text{Furfural Yield} = \frac{N_{\text{furfural}}}{N^0_{\text{xylose}}} \times 100\% \quad (3)$$

The moles of xylose isomers and furfural were calculated by multiplying the molar concentration of each species in a given phase by the volume of that phase. For every phase, except the permeate phase in pervaporation-assisted experiments, the phase volumes were assumed to be equal to their initial values. The volume of permeate was calculated by converting the total permeate mass to volume by assuming a solution density of 1 g mL^{-1}. For reactions conducted at 90 °C with the custom-built apparatus, initial moles were determined from a sample taken from the membrane cell when heating began.

The molar rate of permeation of component i, $\dot{n}_i$, *via* pervaporation is described as follows, using the solution-diffusion model:[43,44]

$$\dot{n}_i = \frac{\Delta m_i}{M_i \Delta t} = A \cdot J_i = A \cdot \frac{P_i}{l}(x_i \gamma_i p_i^{\text{sat}} - y_i p_{\text{permeate}}) \quad (4)$$

where Δm_i is the change in mass of the permeate during the length of time Δt, M_i is the molecular weight, A is the area of the membrane, J_i is the molar flux, P_i is the permeability, l is the thickness of the membrane, x_i is the mole fraction in the liquid feed, γ_i is the activity coefficient in the liquid feed, p_i^{sat} is the saturation vapor pressure at the feed conditions, y_i is the mole fraction in the vapor permeate, and p_{permeate} is the total permeate pressure. Activity coefficients at 90 °C of water (1) and furfural (66) were assumed to be constant, and were estimated from binary water-furfural vapor–liquid equilibrium data.[44] Saturation vapor pressures were determined by the Antoine equation, using constants calculated from binary water-furfural vapor–liquid equilibrium data.[44] Eqn (4) was then used to calculate the membrane permeabilities of water and furfural at 90 °C.

Results and discussion

Experimental studies of reaction at 90 °C

Xylose was converted in the presence of $CrCl_3$ at 90 °C in water. We first discuss the results of batch experiments for three cases: no pervaporation, moderate rate of pervaporation, and rapid rate of pervaporation. A moderate rate of pervaporation refers to use of a 69 μm-thick SDS membrane with a moderate furfural permeance (*i.e.*, permeability divided by membrane thickness) of 1.16 mmol m^{-2} h^{-1} Pa^{-1}, whereas a rapid rate of pervaporation refers to pervaporation with a 4 μm-thick PDMS membrane with a furfural permeance of 5.59 mmol m^{-2} h^{-1} Pa^{-1}. We note that the SDS membrane selectivity (*i.e.*, the ratio of furfural-to-water permeabilities) is 6.3 while that of the PDMS membrane is 1.1; the membrane that enables rapid pervaporation has lower membrane selectivity. The concentrations of furfural in the product (permeate if a membrane was used, otherwise reactor) and reactor were measured as a function of time and these results are shown in Fig. 2a and b.

Fig. 2a shows the cumulative concentration of furfural in the product phase over time for the three experiments. The product concentration collected during the moderate-pervaporation experiment exceeds that of the reaction without pervaporation by approximately an order of magnitude. This demonstrates the benefit of pervaporation-assisted furfural production. Interestingly, the product concentration obtained during the rapid-pervaporation experiment is similar in magnitude to that obtained without pervaporation. This result has two causes. The first is the difference in membrane selectivity: the membrane that enables rapid pervaporation is less selective. The second is not obvious, and reveals a fundamental tradeoff of *in situ* furfural extraction: extraction reduces the furfural concentration in the reactor, which adversely affects the extraction rate of furfural and product purity. This tradeoff is discussed in more detail below.

Fig. 2b shows the concentration of furfural remaining in the reactor as a function of time. The concentrations of furfural decrease in the order of no pervaporation > moderate pervaporation > rapid pervaporation. The permeate furfural concentration is given by:

$$c_{\text{f}}^{\text{perm}} \propto \frac{J_{\text{f}}}{J_{\text{f}} + J_{\text{w}}} \approx \frac{J_{\text{f}}}{J_{\text{w}}} \approx \frac{P_{\text{f}}}{P_{\text{w}}} \frac{x_{\text{f}} \gamma_{\text{f}} p_{\text{f}}^{\text{sat}}}{x_{\text{w}} \gamma_{\text{w}} p_{\text{w}}^{\text{sat}}} \quad (5)$$

A lower furfural concentration in the reactor (x_{f}) diminishes the numerator. In the dilute scenario, as is the case in these experiments (1 g L^{-1} of furfural in water is equivalent to 0.02 mol%), x_{w} is effectively constant. Barring significant changes in activity coefficients, the furfural concentration in the permeate is proportional to the furfural concentration in the reactor. The high concentration of furfural in the permeate during moderate pervaporation (Fig. 2a) is thus directly related to the higher furfural concentration in the reactor (Fig. 2b) and higher membrane selectivity (higher $P_{\text{f}}/P_{\text{w}}$).

The time dependence of xylose conversion and furfural yield, the latter obtained from Fig. 2a and b, are shown in

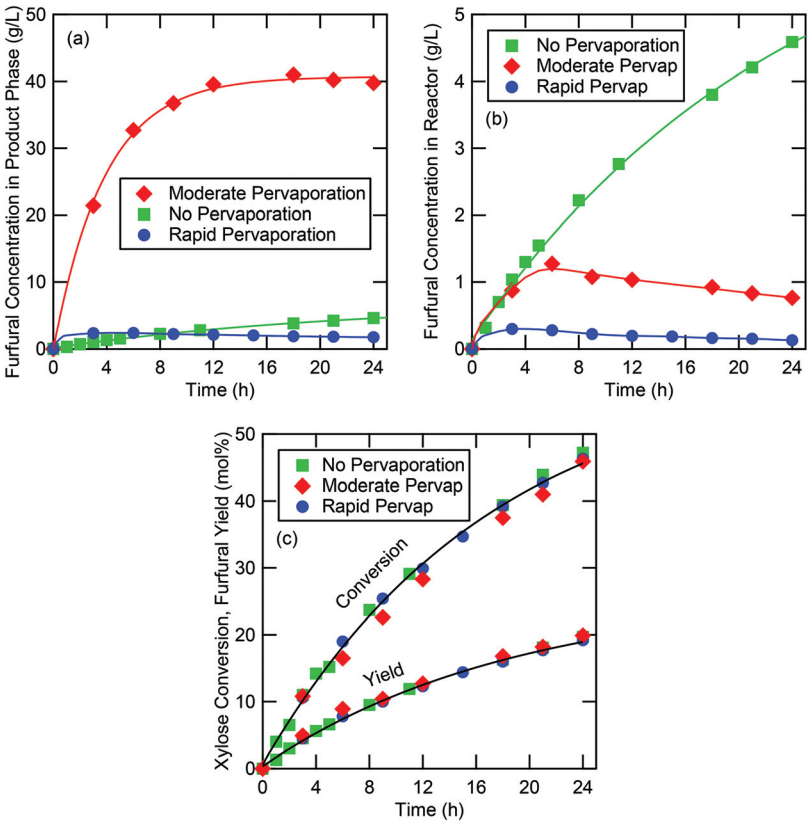

Fig. 2 Batch-mode xylose conversion to furfural at 90 °C with 25 mM $CrCl_3$ with varying rates of pervaporation: none, moderate (69 μm-thick SDS membrane), and rapid (4 μm-thick PDMS membrane). (a) Furfural concentration in product phase (permeate if pervaporation was used, otherwise reactor). (b) Concentration of furfural remaining in the reactor. (c) Xylose conversion and furfural yield. All curves are provided to guide the eye.

Fig. 2c. It is apparent that at 90 °C the rate of pervaporation has no effect on the xylose conversion or the furfural yield. While the distribution of furfural in the different phases is very dissimilar for the three experiments presented in Fig. 2, the total amount of furfural obtained in all three experiments is within experimental error. The data in Fig. 2c suggest that the reaction of furfural to humins does not occur at 90 °C, *i.e.*, Reactions 3 and 5 in Scheme 1 are suppressed at low temperatures. Under these conditions, the main advantage of pervaporation is that the product is more concentrated.

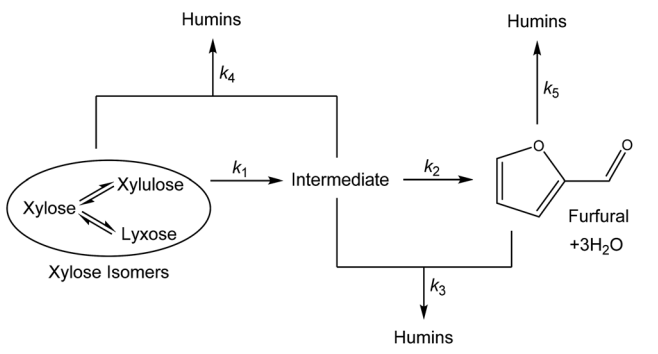

Scheme 1 Reaction network for furfural production from xylose. Isomerization is catalyzed by Lewis acids, while furfural production is catalyzed by Brønsted acids. Insights into this reaction network and characterization of humins can be found in ref. 19 and 46–48.

Perhaps the most interesting finding from these experiments concerns the composition of species crossing the pervaporation membranes. The HPLC and ICP-OES analyses of the permeate samples revealed that only two chemicals were present in the permeate: furfural and water. Neither xylose isomers nor $CrCl_3$ were found above the detection limit (HPLC: ~1 mg L^{-1}, ICP-OES: 0.25 μg L^{-1}); the membranes were perfectly selective for the product (furfural) over the reactants (xylose isomers) and the catalyst ($CrCl_3$). This is because neither xylose isomers nor $CrCl_3$ have a significant vapor pressure and thus should not pervaporate (see eqn (4)). Therefore, pervaporation offers a simple solution to a major challenge in homogeneous catalysis: product/catalyst separation. This finding improves the economic and environmental implications of homogeneous catalysts, which are ubiquitous in current industrial furfural production,[3,7,16,18] and may produce furfural with higher selectivity when compared to heterogeneous catalysts.[42] Additionally, the system described in our study enables the continuous production of furfural with only a small, initial charge of homogeneous catalyst, whereas current industrial methods require constant addition of H_2SO_4.[16,18]

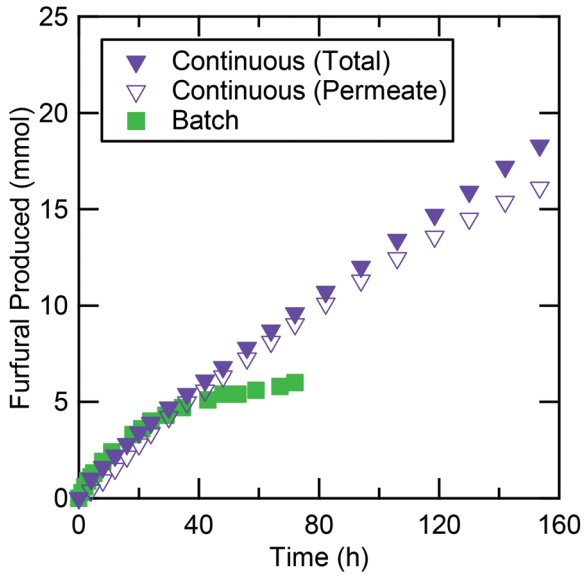

Fig. 3 Continuous-mode furfural production compared to batch-mode production at 90 °C with 25 mM $CrCl_3$. Continuous-mode reaction assisted by 49 μm-thick SDS membrane. Batch-mode reaction conducted without pervaporation. Pervaporation resulted in complete catalyst retention, permitting lack of catalyst addition during continuous reaction.

Fig. 3 compares the amount of furfural produced over time with two reactor configurations: batch and continuous. Both reactions were carried out with the same initial concentration of catalyst. The batch reaction was conducted without furfural pervaporation for 72 h (the results were identical to those achieved with pervaporation, as shown in Fig. 2c). The continuous reaction was conducted by feeding a solution of 100 g L^{-1} xylose in water at a volumetric flow rate matching the pervaporation rate, using a 49 μm-thick SDS membrane. The rate of furfural production is initially rapid in the batch reaction, but slows down significantly after 30 h. By contrast, furfural production is fairly constant throughout the continuous reaction and the amount of furfural produced surpasses that of the batch reaction after about 30 h, even when considering only the permeated furfural, which constitutes about 90% of all of the furfural formed.

Over the course of the continuous experiment, furfural permeability of the membrane decreases while that of water remains constant. This is likely caused by humins interacting unfavorably with the membrane; by the end of the 154 h experiment, a significant amount of insoluble humins formed, making the reaction solution opaque and blanketing the membrane. Further research should be conducted to improve membrane/humins compatibility.

We chose 90 °C for our reaction because the membranes used in this study were not stable at higher temperatures. Operating above 100 °C resulted in the presence of liquid in the permeate upstream of the cold traps, similar in composition to the contents of the cell, suggesting that liquid passed through the membrane; hence, we limited the experiments to 90 °C. This temperature results in the slow conversion of xylose to furfural. Most studies in the field use a reaction temperature of approximately 130 °C.[21–31] We used simulations to explore the performance of a membrane reactor operating at that temperature. There was no difficulty performing the batch experiments without extraction and with liquid–liquid extraction (LLE) at 130 °C. These experiments were performed with 100 mM H_2SO_4 added to the 25 mM $CrCl_3$, as the addition of a Brønsted acid to $CrCl_3$ has previously been found to improve both the reaction rate and the selectivity to furfural.[30] The results of these experiments are shown in Fig. S1 in the ESI.† Under these conditions, *in situ* furfural extraction improved the furfural yield, in contrast with what was found at 90 °C without H_2SO_4 (Fig. 2c). These results are used in the simulations presented below.

Simulations of batch-mode reaction at 130 °C

We fitted a model of the reaction kinetics based on Scheme 1 to the data shown in Fig. S1† in order to determine the reaction rate constants k_1, k_2, k_3, k_4, and k_5. In this scheme, xylose is isomerized to lyxose and xylulose by the Lewis acidity of $CrCl_3$, while these sugars convert to furfural using the Brønsted acidity of both $CrCl_3$ and H_2SO_4. Humins form by condensing the reactive intermediates in this process with the sugars or furfural; humins may also form from furfural alone through a process known as resinification. The intermediates in this process are likely protonated, open-chain sugars, since the protonation has previously been found to be the rate-limiting step.[19,46] We could not measure the pervaporation rates of water and furfural at 130 °C, so we instead measured these rates for SDS membranes from 50 to 90 °C and extrapolated the results to 130 °C. The reaction and pervaporation rate constants can be found in rows 1–7 of Table 1; details are given in the ESI.†

The first simulation undertaken was reaction in the batch mode with furfural pervaporation using an SDS membrane (thickness of 69 μm). The membrane-area-to-reactor-volume ratio, a_v, was varied. The results of these calculations are presented in Fig. 4. The differential equations used for these simulations are given in the ESI.† A value of a_v = 0.17 cm^{-1} corresponds to the geometry of our experimental setup. We also considered two higher values of a_v, 0.58 cm^{-1} and 1.3 cm^{-1}. As expected, furfural yield is a monotonic function of a_v (see Fig. 4a). The furfural concentration in the permeate is a non-monotonic function of time, as shown in Fig. 4b, and the highest concentration is obtained in the reactor with the smallest a_v. This is due to the presence of higher furfural concentration in the reactor. These results present a tradeoff between quantity of furfural produced and concentration of furfural in the permeate.

At first glance, one might assume that the best way to produce furfural in a batch-mode reactor would be to maximize the membrane area, as that would lead to a maximized pervaporation rate and thus minimized furfural concentration in the reactor and minimized furfural consumption by side reactions. However, this is not the case, as shown in Fig. 4 (and Fig. 2, to an extent). Higher values of a_v result in more

Table 1 Parameters used in this study for membrane calculations and simulations

Row	Parameter	Symbol	Value
Reaction rate constants at 130 °C			
1	Xylose isomer dehydration (h^{-1})	k_1	5.1×10^{-1}
2	Furfural production (h^{-1})	k_2	6.1×10^{-1}
3	Furfural-intermediate condensation (L $mmol^{-1}$ h^{-1})	k_3	1.4×10^{-3}
4	Xylose-isomer-intermediate condensation (L $mmol^{-1}$ h^{-1})	k_4	1.2×10^{-3}
5	Furfural resinification (h^{-1})	k_5	5.2×10^{-2}
Additional parameters for simulations at 130 °C			
6	Permeability × activity coefficient for furfural (mol m^{-1} s^{-1} Pa^{-1})	$(P\gamma)_f$	7.9×10^{-10}
7	Permeability × activity coefficient for water (mol m^{-1} s^{-1} Pa)	$(P\gamma)_w$	5.3×10^{-12}
8	Furfural saturation vapor pressure at (kPa)	p_f^{sat}	36.0[a]
9	Water saturation vapor pressure at (kPa)	p_w^{sat}	272[a]
10	Membrane thickness (μm)	l	69
11	Reactor volume (mL)	V	83
12	Xylose concentration of feed solution in continuous-mode reactions (g L^{-1})	$[X]_{in}$	100
13	Xylose isomer molecular weight (g mol^{-1})	M_x	150.13
14	Furfural molecular weight (g mol^{-1})	M_f	96.08
15	Water molecular weight (g mol^{-1})	M_w	18.02
16	Solution density (g mL^{-1})	ρ	1

[a] Ref. 45, saturation vapor pressures (mm Hg) at 75 °C calculated by Antoine equation, $A_{furfural}$ = 8.402, $B_{furfural}$ = 2338.49, $C_{furfural}$ = 261.638, A_{water} = 8.07131, B_{water} = 1730.63, C_{water} = 233.426.

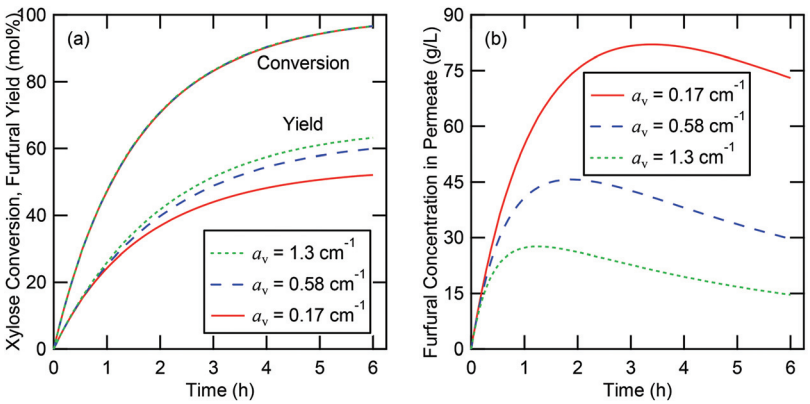

Fig. 4 Simulations of batch-mode xylose conversion to furfural at 130 °C with 25 mM $CrCl_3$ and 100 mM H_2SO_4 with a 69 μm-thick SDS membrane of varying membrane-area-to-reactor-volume ratio, a_v. (a) Xylose conversion and furfural yield. (b) Furfural concentration in the permeate.

furfural produced, albeit at a lower concentration in the permeate. The benefit of the increased yield must be weighed against the cost of purifying the more dilute permeate and using more membrane area.

Simulations of continuous-mode reaction at 130 °C

Simulations were performed using the same initial concentrations as those used in our continuous experiment: the reactor started with 30 g L^{-1} xylose in water and the feed reservoir contained 100 g L^{-1} xylose in water. The differential equations describing this process can be found in the ESI.† The steady-state results of these simulations are plotted as a function of a_v in Fig. 5. The rate at which the xylose solution is fed into the reactor depends on a_v, mainly to balance the rate of permeation of water. Steady state was reached within 50 h of reaction for all values of a_v considered. The main results of interest are the steady-state values of xylose addition rate, furfural permeation rate, concentrations of furfural in the reactor and in the permeate, and reaction selectivity.

Fig. 5a shows the dependence of steady-state xylose addition rate on a_v. The xylose addition rate that can be sustained at a fixed reactor volume is proportional to the total permeation rate, which, in turn, is controlled by the permeation rate of water (the permeate is >95% water). The linear relationship between xylose addition rate and a_v, seen in Fig. 5a, can be anticipated from eqn (4).

Fig. 5b shows the dependence of steady-state furfural permeation rate on a_v. At low values of a_v, furfural produced by reaction is removed by both permeation and side reactions. At high values of a_v, furfural produced by reaction is mainly removed by permeation. The curvature seen in Fig. 5b is due to a cross-over between these two regimes; in the absence of side reactions (*i.e.*, at high values of a_v), the steady-state furfural permeation rate would be a linear function of a_v.

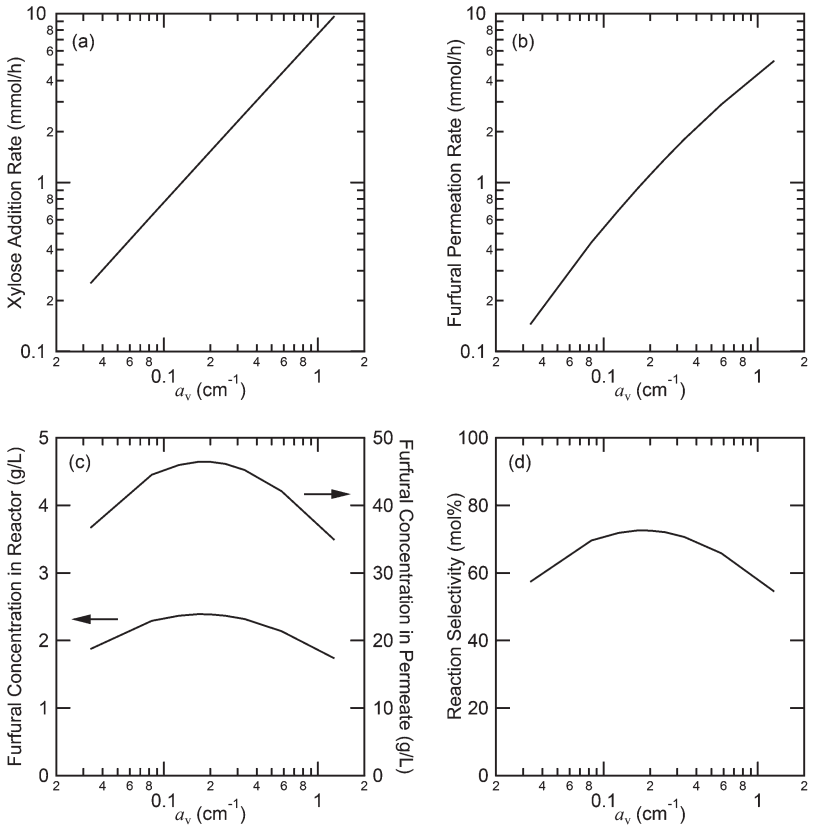

Fig. 5 Simulations of continuous-mode xylose conversion to furfural at 130 °C with 25 mM $CrCl_3$ and 100 mM H_2SO_4 with varying membrane-area-to-reactor-volume ratio, a_v. Plots show steady-state values. (a) Xylose addition rate. (b) Furfural permeation rate. (c) Furfural concentration in the reactor and in the permeate. (d) Reaction selectivity.

In Fig. 5c, we plot the steady-state furfural concentrations in the reactor and in the permeate as a function of a_v. The permeate furfural concentration is proportional to the reactor furfural concentration, as shown in eqn (5). The reactor furfural concentration is determined by balancing the production and disappearance of furfural. Production occurs by reaction and is proportional to xylose concentration in the reactor. Steady-state xylose concentration is determined by balancing xylose addition and xylose consumption by reaction. Addition is proportional to a_v (see Fig. 5a), while consumption is proportional to xylose concentration; thus, xylose concentration is proportional (*i.e.*, linearly related) to a_v. Disappearance of furfural occurs by permeation and consumption through side reactions, and is a slightly non-linear function of a_v because of the diminishing relevance of side reactions with increasing a_v. The dependences on a_v of furfural production and disappearance nearly cancel, resulting in the weak maxima seen in Fig. 5c. The furfural concentrations in the reactor and the permeate are largely insensitive to a_v; a 3700% change in a_v results in a 27% change in furfural concentration. The maxima in Fig. 5c at a_v = 0.17 cm^{-1} are noteworthy as they represent an optimal membrane area if permeate furfural concentration were the parameter being optimized.

Fig. 5d examines the dependence of steady-state reaction selectivity on a_v. We define reaction selectivity as follows:

$$\text{Reaction Selectivity} = \frac{\text{Molar permeation rate of furfural}}{\text{Molar addition rate of xylose}} \times 100\% \quad (6)$$

using data taken from Fig. 5a and b. We obtain a maximum in reaction selectivity at a_v = 0.17 cm^{-1}, which results from the linear dependence of xylose addition rate on a_v and the non-linear dependence of furfural permeation rate on a_v.

The trends presented in Fig. 5c and d suggest that using a_v = 0.17 cm^{-1}, coincidentally the value we had experimentally, yields the best result as that is where the product (permeate) concentration and reaction selectivity are maximized. Of course, the optimized reactor design will depend on many other factors, such as costs of reactants, sale price of furfural, operating costs, *etc*.

Conclusions

A membrane-reactor was built to investigate the dynamics of xylose dehydration and the simultaneous removal of furfural

from the reaction mixture by pervaporation. Both batch and continuous operation of the reactor were implemented. For both modes of operation, $CrCl_3$ was used as the catalyst and the reaction was carried out in water at 90 °C. At this temperature, *in situ* extraction of furfural had no impact on furfural yield in the batch reactor. However, pervaporation increased the concentration of furfural in the permeate by as much as an order of magnitude. More importantly, pervaporation was perfectly selective towards the product (furfural); the concentrations of reactants (xylose isomers) and catalyst ($CrCl_3$) in the permeate stream were below detection limit. Thus, our work demonstrates that pervaporation offers a novel approach for separating products from homogeneous catalysts with negligible vapor pressure, addressing a major downside of homogeneous catalysis when compared with heterogeneous catalysis. This finding improves the economic and environmental viability of homogenous catalysts, which may catalyze more selective furfural production compared to heterogeneous catalysts.[42] Pervaporation also enables continuous operation as a consequence of feeding an aqueous xylose solution to the reactor and pervaporating furfural and water. Doing so allows for the production of furfural in higher quantities than can be achieved by batch-mode operation of the reactor with the same amount of catalyst.

Pervaporation-assisted furfural production was simulated at 130 °C in order to assess the advantages of faster reaction kinetics relative to 90 °C. Simulations of batch-mode operation revealed that increasing the membrane-area-to-reactor-volume ratio, a_v, led to increases in furfural yield and reductions in permeate concentration of furfural. Simulations of continuous-mode operation for different values of a_v led to maxima in reaction selectivity and permeate concentration of furfural at $a_v = 0.17\ cm^{-1}$.

Further experimental studies of membrane-assisted furfural production at temperatures above 90 °C seem warranted. Conducting such experiments will require the development of new pervaporation membranes that are stable at high temperatures.

Conflicts of interest

There are no conflicts of interest to declare.

Acknowledgements

This work was supported by the Energy Biosciences Institute at the University of California at Berkeley, funded by BP. The authors thank Adam Grippo for his assistance in operating the GC-FID for this study and Eric Granlund and Jim Breen of the University of California at Berkeley College of Chemistry machine and glass shops, respectively, for their assistance in constructing the membrane reactor used in this study (Fig. 1).

References

1 R. Mariscal, P. Maireles-Torres, M. Ojeda, I. Sádaba and M. López Granados, *Energy Environ. Sci.*, 2016, **9**, 1144–1189.
2 M. J. Biddy, C. Scarlata and C. Kinchin, Chemicals from Biomass: A Market Assessment of Bioproducts with Near-Term Potential, Report NREL/TP-5100-65509, National Renewable Energy Laboratory, Golden, CO, 2016.
3 A. S. Mamman, J.-M. Lee, Y.-C. Kim, I. T. Hwang, N.-J. Park, Y. K. Hwang, J.-S. Chang and J.-S. Hwang, *Biofuels, Bioprod. Biorefin.*, 2008, **2**, 438–454.
4 G. W. Huber, S. Iborra and A. Corma, *Chem. Rev.*, 2006, **106**, 4044–4098.
5 D. M. Alonso, J. Q. Bond and J. A. Dumesic, *Green Chem.*, 2010, **12**, 1493.
6 A. Corma, O. de la Torre, M. Renz and N. Villandier, *Angew. Chem.*, 2011, **50**, 2375–2378.
7 J. P. Lange, E. van der Heide, J. van Buijtenen and R. Price, *ChemSusChem*, 2012, **5**, 150–166.
8 G. A. Tompsett, N. Li and G. W. Huber, in *Thermochemical Processing of Biomass: Conversion into Fuels, Chemicals and Power*, ed. R. C. Brown, John Wiley & Sons, Ltd, Chichester, UK, 1st edn, 2011, ch. 8, pp. 232–279.
9 J. J. Bozell and G. R. Petersen, *Green Chem.*, 2010, **12**, 539.
10 L. Bui, H. Luo, W. R. Gunther and Y. Roman-Leshkov, *Angew. Chem., Int. Ed.*, 2013, **52**, 8022–8025.
11 D. M. Alonso, S. G. Wettstein and J. A. Dumesic, *Green Chem.*, 2013, **15**, 584.
12 K. Yan, G. Wu, T. Lafleur and C. Jarvis, *Renewable Sustainable Energy Rev.*, 2014, **38**, 663–676.
13 F. B. Oliveira, C. Gardrat, C. Enjalbal, E. Frollini and A. Castellan, *J. Appl. Polym. Sci.*, 2008, **109**, 2291–2303.
14 A. Gandini and M. N. Belgacem, *Prog. Polym. Sci.*, 1997, **22**, 1203–1379.
15 M. Hronec, K. Fulajtarová and T. Liptaj, *Appl. Catal., A*, 2012, **437–438**, 104–111.
16 C. M. Cai, T. Zhang, R. Kumar and C. E. Wyman, *J. Chem. Technol. Biotechnol.*, 2014, **89**, 2–10.
17 I. Agirrezabal-Telleria, I. Gandarias and P. L. Arias, *Catal. Today*, 2014, **234**, 42–58.
18 K. J. Zeitsch, *The Chemistry and Technology of Furfural and its Many By-Products*, Elsevier Science, Amsterdam, 2000.
19 B. Danon, G. Marcotullio and W. de Jong, *Green Chem.*, 2014, **16**, 39–54.
20 J. M. J. Antal, T. Leesomboon, W. S. Mok and G. N. Richards, *Carbohydr. Res.*, 1991, **217**, 71–85.
21 N. K. Gupta, A. Fukuoka and K. Nakajima, *ACS Catal.*, 2017, **7**, 2430–2436.
22 C. García-Sancho, J. M. Rubio-Caballero, J. M. Mérida-Robles, R. Moreno-Tost, J. Santamaría-González and P. Maireles-Torres, *Catal. Today*, 2014, **234**, 119–124.
23 A. Mittal, S. K. Black, T. B. Vinzant, M. O'Brien, M. P. Tucker and D. K. Johnson, *ACS Sustainable Chem. Eng.*, 2017, **5**, 5694–5701.

24 S. Peleteiro, V. Santos and J. C. Parajo, *Carbohydr. Polym.*, 2016, **153**, 421–428.
25 R. Weingarten, J. Cho, J. W. C. Conner and G. W. Huber, *Green Chem.*, 2010, **12**, 1423.
26 H. Li, A. Deng, J. Ren, C. Liu, W. Wang, F. Peng and R. Sun, *Catal. Today*, 2014, **234**, 251–256.
27 M. J. Campos Molina, R. Mariscal, M. Ojeda and M. Lopez Granados, *Bioresour. Technol.*, 2012, **126**, 321–327.
28 S. Le Guenic, F. Delbecq, C. Ceballos and C. Len, *J. Mol. Catal. A: Chem.*, 2015, **410**, 1–7.
29 Y. Wang, F. Delbecq, W. Kwapinski and C. Len, *Mol. Catal.*, 2017, **438**, 167–172.
30 V. Choudhary, S. I. Sandler and D. G. Vlachos, *ACS Catal.*, 2012, **2**, 2022–2028.
31 K. R. Enslow and A. T. Bell, *Catal. Sci. Technol.*, 2015, **5**, 2839–2847.
32 U. K. Ghosh, N. C. Pradhan and B. Adhikari, *Desalination*, 2007, **208**, 146–158.
33 U. K. Ghosh, N. C. Pradhan and B. Adhikari, *Desalination*, 2010, **252**, 1–7.
34 X. Liu, H. Jin, Y. Li, H. Bux, Z. Hu, Y. Ban and W. Yang, *J. Membr. Sci.*, 2013, **428**, 498–506.
35 S. S. Gaykawad, Y. Zha, P. J. Punt, J. W. van Groenestijn, L. A. van der Wielen and A. J. Straathof, *Bioresour. Technol.*, 2013, **129**, 469–476.
36 M. Sagehashi, T. Nomura, H. Shishido and A. Sakoda, *Bioresour. Technol.*, 2007, **98**, 2018–2026.
37 F. Qin, S. Li, P. Qin, M. N. Karim and T. Tan, *Green Chem.*, 2014, **16**, 1262.
38 D. R. Greer, T. P. Basso, A. B. Ibanez, S. Bauer, J. M. Skerker, A. E. Ozcam, D. Leon, C. Shin, A. P. Arkin and N. P. Balsara, *Green Chem.*, 2014, **16**, 4206–4213.
39 D. R. Greer, A. E. Ozcam and N. P. Balsara, *AIChE J.*, 2015, **61**, 2789–2794.
40 A. Wang, N. P. Balsara and A. T. Bell, *Green Chem.*, 2016, **18**, 4073–4085.
41 J. B. Binder, J. J. Blank, A. V. Cefali and R. T. Raines, *ChemSusChem*, 2010, **3**, 1268–1272.
42 R. Weingarten, G. A. Tompsett, W. C. Conner Jr. and G. W. Huber, *J. Catal.*, 2011, **279**, 174–182.
43 J. Wijmans and R. W. Baker, *J. Membr. Sci.*, 1995, **107**, 1–21.
44 R. W. Baker, *Membrane Technology and Applications*, John Wiley & Sons Ltd, The Atrium, Southern Gate, Chichester, West Sussex, P19 8SQ, United Kingdom, 2012.
45 J. Gmehling, U. Onken and W. Arlt, *Vapor-liquid equilibrium data collection*, DECHEMA, Frankfurt, 1978.
46 X. Qian, M. R. Nimlos, M. Davis, D. K. Johnson and M. E. Himmel, *Carbohydr. Res.*, 2005, **340**, 2319–2327.
47 I. van Zandvoort, Y. Wang, C. B. Rasrendra, E. R. H. van Eck, P. C. A. Bruijnincx, H. J. Heeres and B. M. Weckhuysen, *ChemSusChem*, 2013, **6**, 1745–1758.
48 S. Wang, H. Lin, Y. Zhao, J. Chen and J. Zhou, *J. Anal. Appl. Pyrolysis*, 2016, **118**, 259–266.

